

# VEHICLE HULL SHAPE OPTIMIZATION FOR MINIMUM WEIGHT UNDER BLAST LOADING

JJ. Israel<sup>(1)</sup>, H. Tan<sup>(2)</sup>, J.C. Goetz<sup>(3)</sup>, A. Tovar<sup>(1)\*\*</sup>

Matthew P. Castanier<sup>(4)</sup>, Madanmohan V. Vunnam<sup>(4)</sup>, David Gorsich<sup>(4)</sup>

(1) Department of Mechanical Engineering, Purdue School of Engineering and Technology, Indiana University-Purdue University Indianapolis, 723 W Michigan St, SL 260 Indianapolis, Indiana 46202, USA

(2) Mechanical Engineering Department, Manufacturing Research Laboratory, Columbia University, 220 S.W. Mudd Building, 500 West 120th St., New York, NY 10027 USA

(3) Department of Aerospace and Mechanical Engineering, 365 Fitzpatrick Hall of Engineering, University of Notre Dame, Notre Dame, Indiana 46556, USA

(4) U.S. Army Tank Automotive Research, Development and Engineering Center, 6501 E. 11 Mile Road, Warren, Michigan 48397, USA

## ABSTRACT

Shape structural optimization for blast mitigation seeks to counteract the damaging effects of an impulsive threat on occupants and critical components. The purpose of a vehicle energy-deflecting hull is to mitigate blast energies by channeling blast products and high-pressure fluids away from the target structure. Designs of pyramid-shaped protective structures have been proposed in existing and concept vehicle's platforms. These structures are more effective than the traditional flat-plate designs in terms of cabin penetration and weight. Studies on other blast concept design remain scarce. This investigation addresses the design of blast-protective structures from the design optimization perspective. The design problem is stated as to finding the optimum shape of the protective shell of minimum mass satisfying a deformation and envelopes constraints. Performance improvements are observed as the envelope constraint is relaxed and the optimization problem includes a larger number of design variables with the consequent computational cost. In order to consider the solution of a problem with no envelope constraints, this work explores heuristic alternatives: inverted profile and hybrid cellular automata (HCA). Numerical results demonstrate that convergent designs based on trigonometric functions yielded a greater reduction in mass over baseline than all other candidate designs, and show promise for future development. Designs generated via the HCA topography method resulted in structures whose performance paralleled or exceeded most geometrically constrained designs despite the fact that they can be created with fewer computational resources and adapted to irregular design domains.

---

\* Contribution of H. Tan while he was a Graduate Research Assistant at the University of Notre Dame.

\*\* Corresponding author: tovara@iupui.edu

## Report Documentation Page

Form Approved  
OMB No. 0704-0188

Public reporting burden for the collection of information is estimated to average 1 hour per response, including the time for reviewing instructions, searching existing data sources, gathering and maintaining the data needed, and completing and reviewing the collection of information. Send comments regarding this burden estimate or any other aspect of this collection of information, including suggestions for reducing this burden, to Washington Headquarters Services, Directorate for Information Operations and Reports, 1215 Jefferson Davis Highway, Suite 1204, Arlington VA 22202-4302. Respondents should be aware that notwithstanding any other provision of law, no person shall be subject to a penalty for failing to comply with a collection of information if it does not display a currently valid OMB control number.

1. REPORT DATE

**01 MAR 2013**

2. REPORT TYPE

**Journal Article**

3. DATES COVERED

**01-03-2013 to 01-03-2013**

4. TITLE AND SUBTITLE

**VEHICLE HULL SHAPE OPTIMIZATION FOR MINIMUM WEIGHT UNDER BLAST LOADING**

5a. CONTRACT NUMBER

5b. GRANT NUMBER

5c. PROGRAM ELEMENT NUMBER

6. AUTHOR(S)

**J Israel; H Tan; J Goetz; A Tovar; Matthew Castanier**

5d. PROJECT NUMBER

5e. TASK NUMBER

5f. WORK UNIT NUMBER

7. PERFORMING ORGANIZATION NAME(S) AND ADDRESS(ES)

**Department of Mechanical Engineering, Purdue School of Engineering and Technology, 723 W Michigan Street SL 260, Indianapolis, IN, 46202**

8. PERFORMING ORGANIZATION REPORT NUMBER

**; #23737**

9. SPONSORING/MONITORING AGENCY NAME(S) AND ADDRESS(ES)

**U.S. Army TARDEC, 6501 East Eleven Mile Rd, Warren, MI, 48397-5000**

10. SPONSOR/MONITOR'S ACRONYM(S)

**TARDEC**

11. SPONSOR/MONITOR'S REPORT NUMBER(S)

**#23737**

12. DISTRIBUTION/AVAILABILITY STATEMENT

**Approved for public release; distribution unlimited**

13. SUPPLEMENTARY NOTES

**Mechanics Based Design of Structures and Machines**

14. ABSTRACT

**Shape structural optimization for blast mitigation seeks to counteract the damaging effects of an impulsive threat on occupants and critical components. The purpose of a vehicle energy-deflecting hull is to mitigate blast energies by channeling blast products and high-pressure fluids away from the target structure. Designs of pyramid-shaped protective structures have been proposed in existing and concept vehicle's platforms. These structures are more effective than the traditional flat-plate designs in terms of cabin penetration and weight. Studies on other blast concept design remain scarce. This investigation addresses the design of blast-protective structures from the design optimization perspective. The design problem is stated as to finding the optimum shape of the protective shell of minimum mass satisfying a deformation and envelope constraints. Performance improvements are observed as the envelope constraint is relaxed and the optimization problem includes a larger number of design variables with the consequent computational cost. In order to consider the solution of a problem with no envelope constraints, this work explores heuristic alternatives: inverted profile and hybrid cellular automata (HCA). Numerical results demonstrate that convergent designs based on trigonometric functions yielded a greater reduction in mass over baseline than all other candidate designs, and show promise for future development. Designs generated via the HCA topography method resulted in structures whose performance paralleled or exceeded most geometrically constrained designs despite the fact that they can be created with fewer computational resources and adapted to irregular design domains.**

15. SUBJECT TERMS

|                                  |                                    |                                     |  |                                     |                                    |
|----------------------------------|------------------------------------|-------------------------------------|--|-------------------------------------|------------------------------------|
| 16. SECURITY CLASSIFICATION OF:  |                                    |                                     | 17. LIMITATION OF<br>ABSTRACT<br><b>Public Release</b> | 18. NUMBER<br>OF PAGES<br><b>27</b> | 19a. NAME OF<br>RESPONSIBLE PERSON |
| a. REPORT<br><b>unclassified</b> | b. ABSTRACT<br><b>unclassified</b> | c. THIS PAGE<br><b>unclassified</b> |  |                                     |                                    |

**Standard Form 298 (Rev. 8-98)**  
Prescribed by ANSI Std Z39-18

## NOMENCLATURE

|                       |  |
|-----------------------|--|
| $a_1, a_{21}, a_{22}$ | Trigonometric function coefficients            |
| $c$                   | Element thickness                              |
| $\mathbf{d}$          | Vector of design variables                     |
| $\mathbf{e}$          | Vector of error values                         |
| $f_1, f_2$            | Trigonometric function coefficients            |
| $h$                   | Structure height                               |
| $q$                   | Nodal location after blast                     |
| $r$                   | Radial coordinate of surface of revolution     |
| $t$                   | Time variable                                  |
| $\mathbf{x}$          | Vector of $x$ -coordinate values for all nodes |
| $\mathbf{y}$          | Vector of $y$ -coordinate values for all nodes |
| $y$                   | Deflection after blast                         |
| $\mathbf{z}$          | Vector of $z$ -coordinate values for all nodes |
| $C_0, C_1, C_2, C_3$  | Polynomial function coefficients               |
| $M$                   | Mass function                                  |
| $N$                   | Number of free nodes in the design space       |
| $P_c$                 | Cabin penetration function                     |
| $P_{c \max}$          | Maximum allowable penetration                  |
| $R$                   | Radius of surface of revolution                |
| $S$                   | Envelope constraint function                   |
| $\alpha$              | Gaussian spread variable                       |
| $\delta$              | Gaussian height variable                       |
| $\rho$                | Element density                                |

## 1 INTRODUCTION

This article investigates the automated design process of isotropic plates to mitigate the effects of blast loading. Framed against the problem of blast protection system design for vehicle applications, the performance of the designs is measured in terms of mass and deflection, as has been done in previous investigations of lightweight armor design [1]. There has been substantial work on analysis of the effects of blast loading on shell structures. Argod and Belegunda have shown significant improvement of structure design using velocity-field based optimization and have demonstrated the effects of different boundary conditions for plates of this kind [2]. Methods of blast energy absorption have been evaluated through extensive design investigations of composite materials [3] [4], as well as numerical [5] and experimental [6] simulations of sacrificial structures.

Physical nonlinearities are abundant in the process of a blast event. In such events, the kinetic energy is transferred to the structure by means of a fluid structure interaction. The dynamics of the events and their interactions with solid structures is an area that has been extensively researched [7]. The governing equations of thermo-mechanics that characterize blast loading conditions require the conservation of mass and energy, balance of linear and angular momentum, heat

equations, stress/strain relations, and, in the case of blast pressure calculations and shrapnel penetration calculations, kinetic and caloric equations of state; Kinetic and caloric equations of state are required in solving the behavior of pressurized gases upon detonation, volumetric equations of state may be used to solve for the behavior of the target ceramic material. From this basic thought process, it appears that in order to solve for the behavior of the target material while accounting for all the thermo-mechanical interactions of the blast wave and projectile impacts, the solution of all sixteen equations are required. To reduce the total governing equations required, it may be necessary to simplify or dissect the phenomena of detonation into more manageable models.

Several experimental investigations have been conducted in the field of detonation events [8]. The CONWEP model developed by the Army Research Laboratory, and currently used in commercial finite element blast simulations, is considered adequate for use in engineering studies of vehicle response to the blast from land mines [7]. The CONWEP algorithm does not explicitly simulate the effects of the detonation reaction with air nor does it calculate the shock wave propagation and its reactions with the target structure. In continuum mechanics the Arbitrary Lagrange-Eulerian method is commonly applied in the finite element analysis of fluid structure interactions. The ALE method is popular in its application to large shear deformations where a traditional Lagrangian mesh breaks down due to geometric instabilities. Compared to a traditional Eulerian mesh such as those used in computational fluid dynamics analysis, the ALE method is better suited to tracking fluid boundaries and resolving flow details involving large volume changes [9]. Due to the importance of fluid structure interactions in many engineering applications, the ALE algorithm has been applied to commercial finite element solvers and is currently available in the LS-DYNA 971 release.

The length and time scales in blast analysis are very different from that of the traditional linear elastic quasi-static optimization problems. In such previously studied problems the material stress strain relations are assumed to follow linear elastic models for quasi-static problems and linear plastic deformation relations are assumed for material yielding under dynamic simulations. Materials in the design domain are generally assumed to be isometric and the density of the material is assumed to be controllable and linearly proportional to the material properties. The blast optimization problem proposed involves pressure and mechanical loading conditions that cannot be properly modeled using the existing linear elastic material models. The time scale involved under blast loading conditions involves irreversible processes that require a more complete model of thermal mechanical reactions than that currently available. Of primary concern in the detonation and explosion interaction event as opposed to a crash event is the interaction of the blast shock wave with the target structure.

The fundamental optimization problem to be analyzed in the design of a structure for blast mitigation is that of minimizing the kinetic energy transfer from the blast wave to the solid body. The goal of such efforts is to develop a system that could absorb a significant amount of the energy released in a blast event such that the underlying structure may be preserved. This article will instead focus on various design techniques for isotropic plate structures within the same design

space, and subject to the same objective function and constraints in order to compare design methodologies in terms of optimized structures produced via formal optimization techniques such as sequential quadratic programming (SQP) and hybrid cellular automata (HCA). The objective of this investigation is to compare feasible design methodologies through the expansion of the problem dimension in order to reach the limits of performance. For the purposes of this study, seven profiles are evaluated, each under the same loading and boundary conditions.

The candidate profiles are divided into two broad categories: geometrically constrained design (GCD) and free shape design (FSD). A GCD includes an analytical description of the structure's profile in the problem statement, while FSD such expression such constraint is relaxed. The small number of design variables describing the structure's profile in a GCD allows the use of traditional programming methods such as sequential quadratic programming. In the case of FSD the use of such traditional methods is impractical; therefore, this work makes use of heuristic approaches, i.e., inverted profile and hybrid cellular automata.

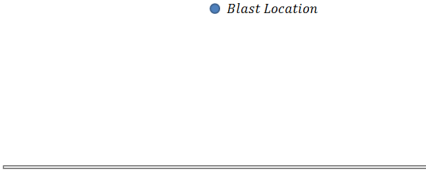
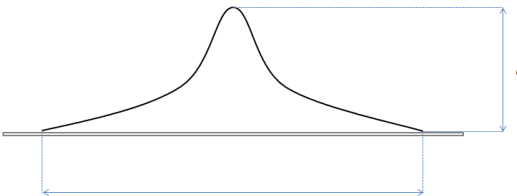
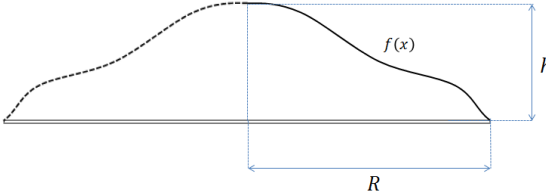
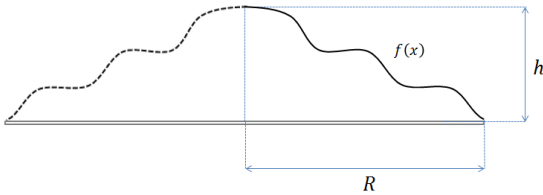
## 2 PROBLEM DEFINITION

In blast protection system design for vehicle applications, there are two primary performance measures of critical relevance: weight and cabin penetration. Weight is privileged as a key performance measure stemming from the need for lightweight, compact structures that can be fitted to existing vehicle designs without extensive re-design of the frame or other vehicle systems. The goal is to design light structures that do not adversely affect vehicle performance. Large deflections of the plate structure due to a blast event can cause penetration into the passenger cabin of the vehicle and result in occupant injury. In this way, cabin penetration can be seen as a means of quantifying the degree to which the blast energy has been mitigated; if the deflection of the plate structure post-blast exceeds a certain amount, the design is unsuccessful. In consideration of these performance measures, the objective function is formulated as the mass of the plate structure and is minimized subject to displacement constraints (cabin penetration) and design space limitations. The general optimization problem addressed in this paper is

$$\begin{aligned}
 & \text{find} && \mathbf{d} \\
 & \text{minimize} && M(\mathbf{d}) \\
 & \text{subject to} && P_c(\mathbf{d}) - P_{c \max} \leq 0 \\
 & && S(\mathbf{x}, \mathbf{y}, \mathbf{z}, \mathbf{d}) = 0 \\
 & && \mathbf{d}^L \leq \mathbf{d} \leq \mathbf{d}^U
 \end{aligned} \tag{1}$$

where  $\mathbf{d} \in \mathbb{R}^n$  is the set of all design variables characterizing the shape and thickness of the plate,  $M(\mathbf{d})$  is the plate's mass,  $P_c(\mathbf{d})$  is the penetration after the blast event with respect to datum plane,  $P_{c \max}$  is the maximum allowable value for penetration. The envelope constraint  $h(\mathbf{x}, \mathbf{y}, \mathbf{z}, \mathbf{d})$  is a function of the nodal coordinates  $\mathbf{x}$ ,  $\mathbf{y}$ , and  $\mathbf{z}$ . The box constraint  $\mathbf{d}^L$  and  $\mathbf{d}^U$  are the lower and upper bounds for the design variables, respectively. The envelope constraint  $h$  is progressively relaxed so the design space is expanded to contain more design variables. This allows increasing the performance design problem at expenses of more complex topographies. This work is framed in the context of vehicle protection from blast events. Five envelope constraints are considered in this work (Table 1).

**Table 1: Envelope constraints and corresponding number of design variables**

| Envelope constraint        | Schematic  | Num. of design variables |
|----------------------------|--|--------------------------|
| Flat Plate                 |  <p style="text-align: center;">● Blast Location</p>    | 1                        |
| Pyramid Profile<br>Pyramid |  <p style="text-align: center;">● Blast Location</p>   | 2                        |
| Gaussian                   |  <p style="text-align: center;">● Blast Location</p> | 3                        |
| Polynomial                 |  <p style="text-align: center;">● Blast Location</p> | 5                        |
| Trigonometric              |  <p style="text-align: center;">● Blast Location</p> | 6                        |

- **Flat Plate Design.** This topography for flat plane is defined by the condition in which the all the  $z$  –coordinate values for every node is the same. This design is regarded as the baseline for comparison with each progressive candidate design.
- **Pyramid Profile Design.** Methods of blast mitigating structure design have been evaluated extensively through experimental efforts in the development of lightweight V-shaped hulls, and have demonstrated that V-shaped designs can mitigate the effects of blast events [10]. The pyramid profile design is an improvement of the V-shape design used in concept designs, due to the fact that it is constrained on four sides.
- **Gaussian Function Design.** In the interest of creating more complex curves through minimal expansion of the design domain, a plate structure that takes on the shape of a Gaussian function of two variables is generated. Previous explorations of this shape demonstrated promising, yet inconclusive results [11].
- **Polynomial Function Design. And Trigonometric Function Design.** Two additional design methodologies are examined which relax the problem further. In both the polynomial function and trigonometric function cases, a function of several variables is used to generate a complex curve. The plate design is achieved as a surface of revolution by rotating the curve about the  $z$  –axis.

As the number of design variables increases, so does the complexity of the analytical description of each design. A large increase in the number of design variables makes the problem intractable in that an analytical solution for sensitivity has not been derived. In short, for traditional sensitivity-based design optimization, the cost of sensitivity limits the number of design variables. In order to overcome those limitations, two alternative methods are examined which utilize a large design domain and rely on user input to avoid intractability. These free shape designs deal with the most relaxed problem, as there is no underlying analytical description of the shape:

- **Inverted Profile Design.** There has been some interest in creating a plate that takes on an inversion of the topography of a flat plate after a blast event, largely inspired by the mathematical idea of the catenary curve, the idealized shape that a chain assumes under its own weight. The reasoning being that the complex blast pressure distribution would then determine the shape of the plate and influence the  $z$ -coordinate at each node proportional to the magnitude of the loading. This approach has been utilized in the design of bridges as well as in the world of architectural design [12, 13].
- **HCA Topography Design.** The Hybrid cellular automata method, or HCA, is an approach that allows us to handle many design variables. In this approach, the field variable, in this case the nodal  $z$  –coordinate, is driven toward a pre-determined set point. HCA methods have been used in the past by Goetz and Tovar to develop two-material topologies for blast mitigation [1] , but there is a need to demonstrate the uses of HCA for topography optimization.

## MODELING CONSIDERATIONS

### 2.1 Design Domain

The design domain, which defines the envelope constraints and boundary conditions for the problem, is chosen in such a way as to simulate under-vehicle conditions. Consider the vehicle model shown in Figure 1.

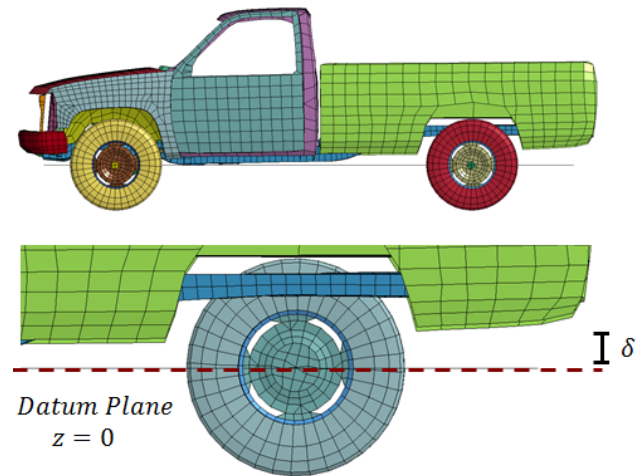


**Figure 1: Truck model for design space development (top) and detail of under-vehicle showing datum plane (bottom)**

The design domain is chosen as a three dimensional space of the same dimensional order as the vehicle model shown in the figure, where the datum plane (shown as the dotted line) is an arbitrary distance  $\delta = 0.03 \text{ m}$  from the upper plane of the design space to account for the distance between an under-vehicle plate structure and the passenger cabin. This distance allows for some penetration below the datum plane without penetrating the cabin.

In order to privilege the display of the optimized plate designs, the design domain has been modeled from beneath or “upside down” orientation, resulting in a 1 m by 1 m by 0.15 m three-dimensional space with the datum plane distance  $\delta$  from the bottom plane as shown in Figure 2. For this orientation, a node is considered to penetrate the cabin if its nodal  $z$  –coordinate is less than  $-0.03 \text{ m}$ .

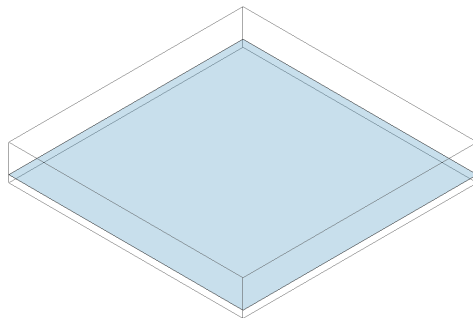


**Figure 2: Design domain representation with datum plane ( $z = 0$ ) shown.**

The penetration is taken as the z-displacement relative to the initial position. The thickness of the plate,  $c$ , is computed as the sum of the distance between the through-integration points for the shell elements. For all models, shell elements with five through thickness integration points are used. In some design candidate cases, the nodal locations are determined as a function of additional design parameters. Additional design parameters are shown on a case-by-case basis below.

## 2.2 Baseline Design and Mesh Refinement

The baseline design, which serves as a starting shape for the optimization methods, is a flat, isotropic steel plate with the following characteristics:

- Uniform thickness: each element has the same through thickness based on the distance between integration points.
- Fixed on all sides: all degrees of freedom are constrained for all nodes at the sides of the plate. These boundary conditions have been demonstrated to have quantitatively the same z –displacement response over time as a free plate with a stiffener support around the edge [2]. This is meant to simulate a plate capable of maintaining rigidity at the edges and approximate conditions in vehicle design.

The plate is modeled using four node shell elements with five through thickness integration points. Mesh density studies showed that the z –displacement was relatively insensitive to mesh refinement. In order to preserve computational efficiency, the plate was modeled with a coarse mesh grid of 26 by 26 nodes, for a total of 625 elements, as shown in Figure 3.

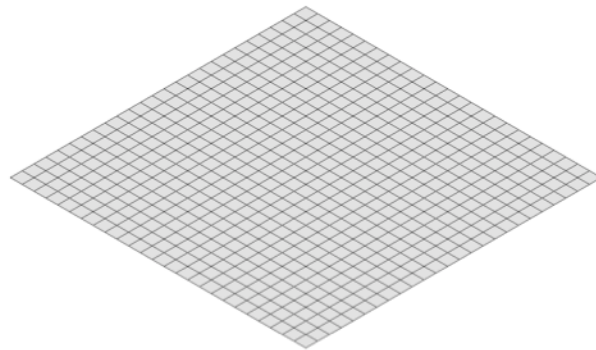


*Figure 3: Baseline design 26 x 26 node plate.*

The plate is modeled as A36 type structural steel with linear elastic-plastic behavior – LS-DYNA input card \*MAT\_PIECEWISE\_LINEAR\_PLASTICITY. The following material properties are used in each design case: mass density 7800 kg/m<sup>3</sup>, Young’s modulus 200 GPa, Poisson’s ratio 0.3, yield stress 220 MPa, tangent modulus 2 GPa.

## 2.3 Loading Conditions and Time Considerations

The loading conditions were applied using the ConWep BLAST\_ENHANCED engineering model of an air blast, with the same set of parameters used consistently throughout to ensure continuity for comparative purposes: charge magnitude = 5 kg TNT, charge location = 40 cm above the center of

the plate (0, 0, 0.4), type of blast source = spherical free-air burst (LS-DYNA keyword input – BLAST=2). The peak pressure loading  $P_0$ , as shown in Figure 4, occurs very quickly after the initial detonation time and the maximum z-displacement occurs as a result of this pressure [14]. Thus, a very small simulation time ( $t \leq 0.0055$  s) was chosen. Exact simulation time for each design was chosen on a case-by-case basis.

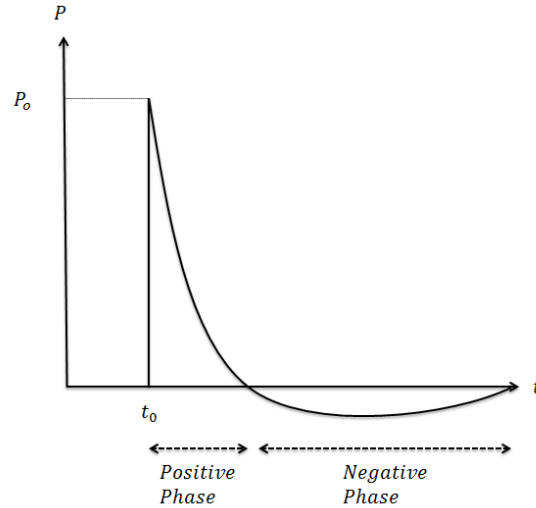


**Figure 4: Blast pressure time history.**

## 2.4 Adaptation of Optimization Problem

Each candidate design is considered individually and adapted to the existing optimization problem as the number of design variables in  $\mathbf{x}$  increases. In each case the objective function and the bounds on  $\mathbf{d}$  are different, but the penetration constraints and envelope are the same case in each:

- Penetration constraint:  $P_c(\mathbf{d}, t) - P_{c \max} \leq 0$   
 $P_{c \max} = 0.03$  is chosen to ensure that the optimized topography results in a design where the lowest  $z$  –coordinate after the blast event is -0.03 m, i.e., there is no cabin penetration.
- Design domain constraint:  $\mathbf{z}^L \leq \mathbf{z} \leq \mathbf{z}^U$   
 $\mathbf{z}^L = -0.03$  m and  $\mathbf{z}^U = 0.12$  m are chosen to ensure that the design does not violate the domain constraints.

## 2.5 Approximation of Surface Area

For a given surface of two variables, the area can be determined analytically according to the following equation:

$$\iint \sqrt{1 + \left(\frac{\delta}{\delta x} f(x, y)\right)^2 + \left(\frac{\delta}{\delta y} f(x, y)\right)^2} \delta x \delta y \quad (2)$$

For complicated surface geometry whose functions involve non-linear equations of several variables as the ones examined here, analytical methods of determining the surface area of the plate become problematic. Instead, the surface area of the plate is approximated based on nodal locations.

If we consider a single element as shown below in Figure 5, we can define vectors that begin and end on the nodes associated with each element.

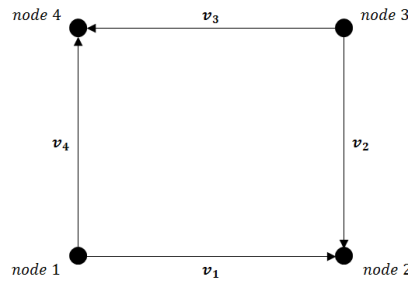


**Figure 5: Vector numbering to determine element area.**

For a given surface divided into  $N$  elements, the surface area can be described as in (3) where a new set of vectors is generated for each element ( $k$ ) based on nodal coordinate information.

$$A \cong \sum_{k=1}^N \frac{1}{2} \|v_1^k \times v_2^k\| + \frac{1}{2} \|v_3^k \times v_4^k\| \quad (3)$$

Mass calculations based on this method of approximating surface area were compared to the mass results generated by the LS-DYNA internal method and were found to be within  $\pm 1\%$  in nearly all cases.

### 3 GEOMETRICALLY CONSTRAINED DESIGNS

In addition to the baseline design, three additional design candidates are developed using for the optimization problem as described in the proceeding sections. All benchmark candidate optimization problems are solved using an active set algorithm. The non-linear programming algorithm is described by Powell [15] and incorporated in Matlab.

#### 3.1 Flat Plate Design

The baseline for all candidate design comparisons is a plate in which all nodal locations are initially zero. The objective function is a single variable function in which only the thickness  $c$  of the plate is varied until the constraints are satisfied. The optimization problem for the flat plate candidate design is:

$$\begin{aligned} &\text{find} && c \\ &\text{minimize} && M(c) = \rho A c \\ &\text{subject to} && P_c(c) - P_{c \max} \leq 0 \\ &&& \mathbf{z} = \mathbf{0} \\ &&& 7.5 \text{ mm} \leq c \leq 50 \text{ mm} \end{aligned} \quad (4)$$

The thickness of the plate is computed as constant at every node. Initial  $z$ -coordinate values are uniform for the initial surface, i.e., all pre-blast nodal locations  $\mathbf{z} = \mathbf{0}$ . The  $P_{c \max}$  value allows the plate to deflect a small amount while still satisfying the constraints, but the optimized design exhibits a relatively large increase in mass in order to absorb the blast wave while ensuring that the deflection constraint is satisfied. This result illustrates the problem associated with the up-

armoring of vehicles using only thick, flat plate structures: the large increase in vehicle mass associated with ensuring an appropriate level of protection is often enough to cause other vehicle-performance issues. The mass characteristics of all proceeding designs are compared to this result as a measure of design performance. The results of the active set method optimization are thickness  $c = 29.2$  mm with a corresponding mass  $M = 226.4$  kg.

### 3.2 Pyramid Profile Design

There are well-documented studies that demonstrate the ability of v-shaped plate structures to deflect/absorb the energy from a blast event. This candidate design is meant to emulate that V-shaped profile in rendering a symmetric pyramidal design for optimization. As the base of the pyramid is fixed at all constrained nodes, the analytical description for the plate structure is a function of the height of the structure. The number of design variables for this method is increased to two: the height of the structure and the thickness of the plate are optimized. After the profile generation procedure, the plate takes on a pyramid profile where the height  $h$  and thickness  $c$  of the plate are allowed to vary and is optimized with the objective function as a two variable function as

$$\begin{aligned}
 & \text{find} && c, h \\
 & \text{minimize} && M(c, h) = 2 \rho c \sqrt{h + 1/4} \\
 & \text{subject to} && P_c(c, h) - P_{c \max} \leq 0 \\
 & && z - \frac{h}{0.5} x + h = 0 \\
 & && 7.5 \text{ mm} \leq c \leq 50 \text{ mm} \\
 & && 0 \text{ mm} \leq h \leq 120 \text{ mm}
 \end{aligned} \tag{5}$$

Preliminary results showed that the pyramid tends toward the maximum allowable height; therefore, the maximum height of the design was chosen as 120 mm for the optimization in order to ensure that the envelope constraints were not violated. Convergent results demonstrate an increase in height to the boundary of the design domain while exhibiting a thickness less than half of that of the baseline design, resulting in a structure of significantly smaller mass.

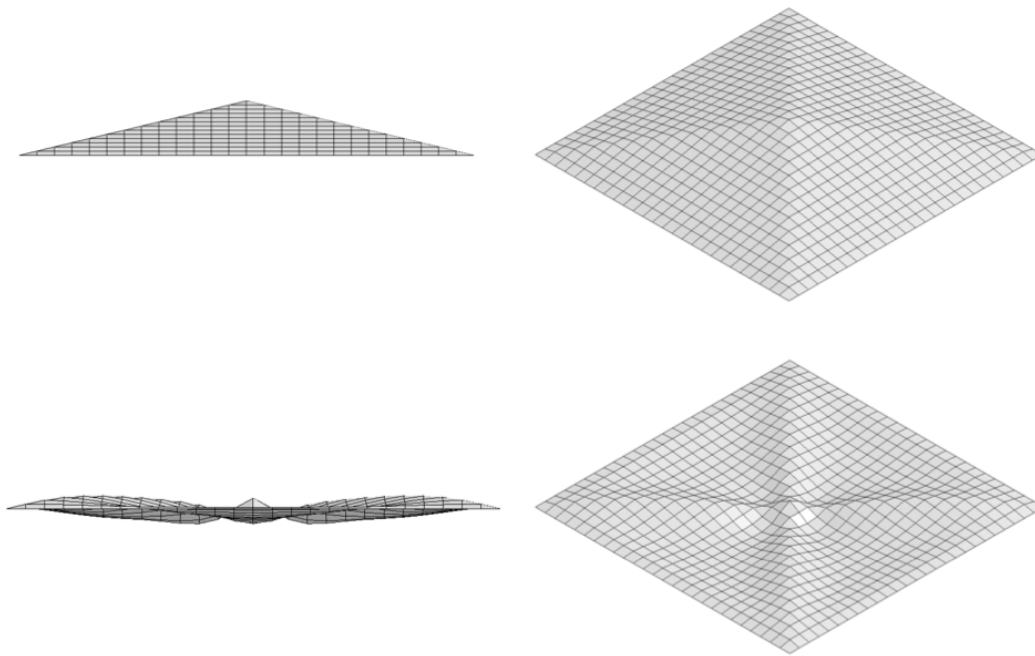


**Figure 6: Finite Element model showing the optimized pyramid profile design before (top) and after a blast event (bottom). Convergent numerical results: thickness = 12.4 mm, height = 120 mm, and mass = 99.1 kg.**

As can be seen Figure 6, the blast deforms the structure in such a way that the pyramid structure is nearly flattened, but the deflection of the plate in the z-direction is within the allowable tolerance.

### 3.3 Gaussian Function Design

Continued investigation of designs with more complex curvature led to the development of a plate structure with topography that conforms to the surface described by a Gaussian function of two variables. The common single variable equation for a Gaussian function is given as

$$f(x) = a \exp\left[-\frac{(x-b)^2}{2c^2}\right] \quad (6)$$

where  $a$ ,  $b$ , and  $c$  are all constants. In three-dimensional space, given a mesh grid of  $x$  and  $y$  values, we can define a surface that is described by the equation

$$f(x,y) = \delta \exp\left[-\left(\frac{(x-x_0)^2}{\alpha} + \frac{(y-y_0)^2}{\alpha}\right)\right] \quad (7)$$

where  $\delta$  is the height of the surface,  $\alpha$  is a constant related to the spread of the bulge in the center. The curve is centered as point  $(x_0, y_0)$ . This allows us to optimize a plate structure that can take on complex curvatures, while allowing the use of the common optimization problem used throughout and only increasing the dimensional order of the design problem by one.

After the profile generation procedure, the plate takes on a Gaussian profile where  $\alpha$  and  $\delta$  and thickness of the plate are allowed to vary and is the design is optimized with the objective function as a function of the three variables  $c$ ,  $\alpha$ , and  $\delta$  to as

$$\begin{aligned}
& \text{find} && c, \alpha, \delta \\
& \text{minimize} && M(c, \alpha, \delta) = \rho c A(\alpha, \delta) \\
& \text{subject to} && P_c(c, \alpha, \delta) - P_{c \max} \leq 0 \\
& && z - \delta \exp \left[ - \left( \frac{(x - x_0)^2}{\alpha} + \frac{(y - y_0)^2}{\alpha} \right) \right] = 0 \\
& && 7.5 \text{ mm} \leq c \leq 50 \text{ mm} \\
& && 0 \leq \alpha \leq 1 \\
& && 0 \leq \delta \leq 0.12
\end{aligned} \tag{8}$$

The optimized shape before and after blast events is shown in Figure 7, The design exhibits deformational characteristics similar to the pyramid profile design in that is nearly flattened by the blast pressure while deflecting/absorbing enough of the energy to allow only a small amount of deflection in the negative  $z$  –direction.

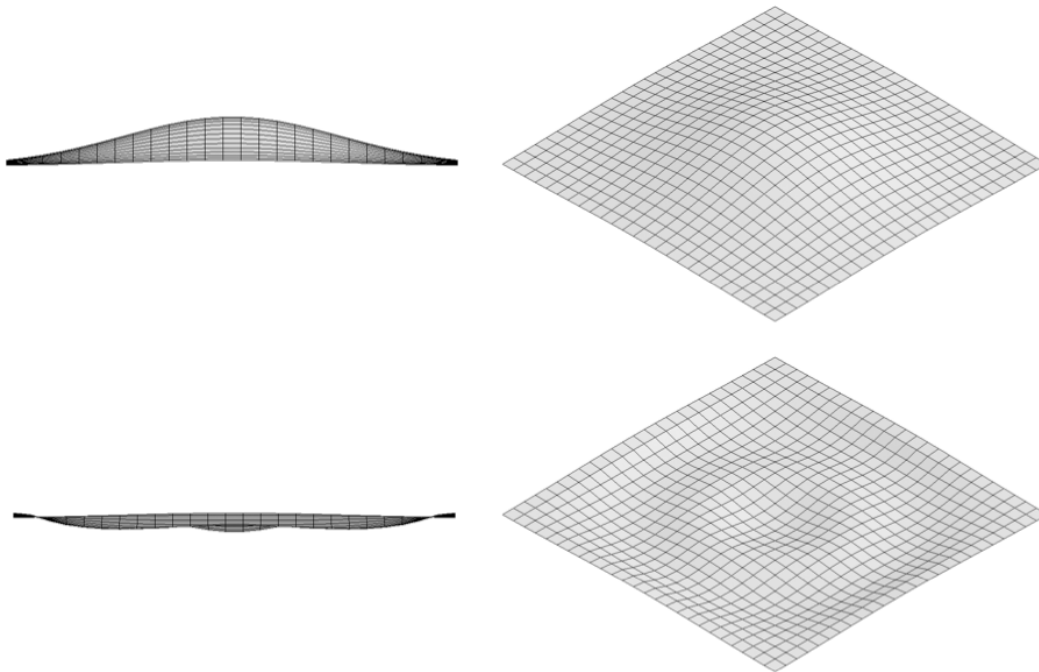


**Figure 7: FE model showing the optimized Gaussian profile design before (top) and after a blast event (bottom). Convergent numerical results: thickness = 11.8 mm,  $\alpha = 0.099$ ,  $\delta = 0.12$ , mass = 94.3 kg.**

The mass of the convergent design is significantly lower than that of the baseline design ( -58.4 %) and improves upon the mass reduction exhibited by the pyramid profile design by a small margin ( -4.84 %). In this case, an increase in the number of design variables resulting in a more complex shape also yielded a more successful design.

### 3.4 Polynomial Function Design

In the interest of creating more complex curved surfaces that could be controlled through the variation of only a few variables and increase the dimension of the problem further, a method for

generating plate structures that take on a 3<sup>rd</sup> order polynomial curve was developed. Given the design space as stated above, a 3<sup>rd</sup> order polynomial curve is assumed to begin at some height (h) at the center of the plate and end at a height of zero at some distance (R) from the center. The polynomial function can then be used to generate a surface by rotating the curve about the z-axis. It should be noted that this method does not make use of the entire square design domain of the plate but instead utilizes a radial design domain extending from the center of the plate.

Starting with a third order polynomial equation

$$f(x) = C_0 + C_1x + C_2x^2 + C_3x^3 \quad (9)$$

we apply our boundary conditions stated above as equality constraints in the optimization problem, which results in a plate design method as a function of five variables: the four polynomial coefficients and the thickness of the plate. This in turn increases the dimension of the problem to five and the plate takes on a polynomial profile, which can be optimized as a function of five variables:

$$\begin{aligned} & \text{find} && c, C_0, C_1, C_2, C_3 \\ & \text{minimize} && M(c, C_0, C_1, C_2, C_3) = \rho A(C_0, C_1, C_2, C_3) c \\ & \text{subject to} && P_c(c, C_0, C_1, C_2, C_3) - P_{c \max} \leq 0 \\ & && x_i^2 + y_i^2 = r_i^2 \\ & && z - C_0 + C_1r + C_2r^2 + C_3r^3 = 0 \\ & && h = 120 \text{ mm} \\ & && 7.5 \text{ mm} \leq c \leq 50 \text{ mm} \\ & && C_0 - h \leq 0 \\ & && C_0 + RC_1 + R^2C_2 + R^3C_3 = 0 \end{aligned} \quad (10)$$

The optimized shape before and after blast events is shown in Figure 8 and similarly to the previous candidate designs, the plate structure exhibits deformation characteristics in which the structure is nearly flattened by the blast, while allowing only a small amount of deflection in the z-direction below the datum plane, within the tolerance of the penetration constraint. The optimized design is an improvement over the baseline design in terms of mass reduction, but demonstrates an increase in comparison to the pyramid profile and Gaussian profile designs due to an increase in thickness in the converged results. It is thought that this increase in thickness is in compensation for a feature of this design not present in the previous two design methods mentioned here. Due to the fact that the design is generated as a surface of revolution, which is inherently circular, while the shape of the plate as described by the domain is square; the whole design domain is not used on the generation of the plate profile. In turn, this creates an inherent weakness in the plate structure in the portion of the plate beyond the area described by the surface of revolution – i.e. the flat portions of the plate outside of the bulging center portion.

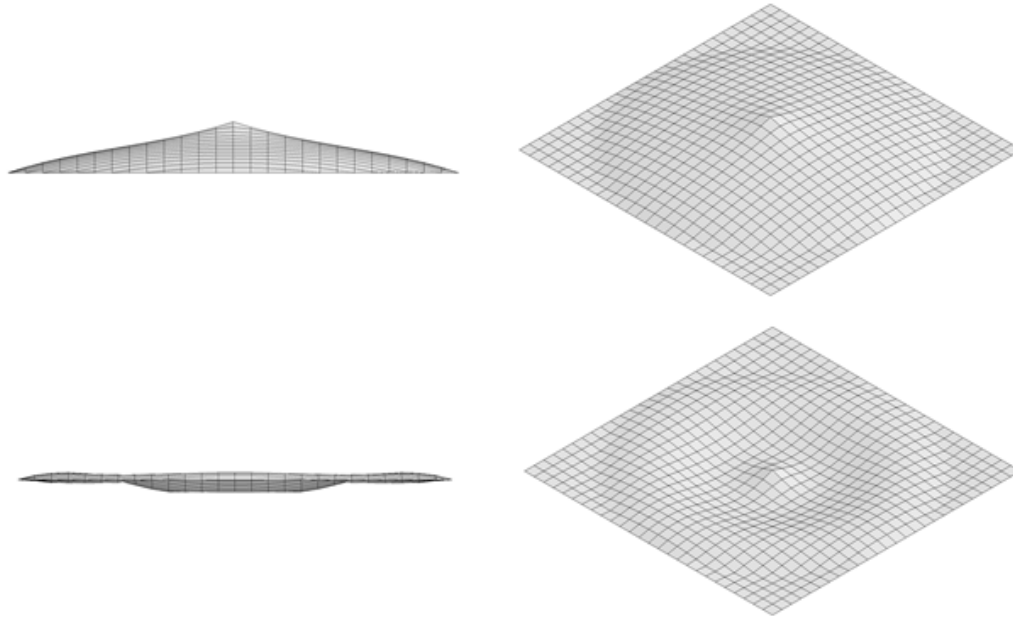


**Figure 8: Finite Element model showing the optimized polynomial function surface design before (top) and after a blast event (bottom). Convergent numerical results: thickness = 14.1 mm,  $C_0 = 0.112$ ,  $C_1 = -0.332$ ,  $C_2 = 0.642$ ,  $C_3 = -0.859$ , mass = 113.1 kg.**

### 3.5 Trigonometric Function Design

The trigonometric function design was developed in an effort to explore a design whose surface exhibits a more complex curvature than a 3<sup>rd</sup> order polynomial without substantially raising the dimension of the design problem. Although the polynomial design did not demonstrate an increase in performance correlated to an increase in problem dimension, this design allows a dramatic increase in curvature complexity with only a marginal increase in the problem dimension. While the shape generation process is very similar to the one used in the polynomial function design, the surface of revolution is based on the sum of a set of oscillating functions, namely *cos* and *sin*. Through the definition of a few coefficients, this function allows for curvature that could only be represented by a very high-order polynomial function. Similar to the polynomial design method described above, this method does not make use of the entire square design domain of the plate but instead utilizes a radial design domain extending from the center of the plate.

Given the design space as stated above, a curve is assumed to begin at some height (*h*) at the center of the plate and end at a height of zero at some distance (*R*) from the center. We define *f(x)* as the sum of a *cos* and *sin* function with coefficients to allow customization of the curve within the design domain:

$$f(x) = C_0 \cos C_1 x + C_2 \sin C_3 x \quad (11)$$

After some development, the coefficients are chosen to allow the designer to control overall height and width of the structure and allow for some amplitude and frequency modulation of the second term to generate a wave shape. This would allow for the creation of plate structures of much

greater complexity than a 3<sup>rd</sup> order polynomial. The coefficients in the equation above become the design variables and the trigonometric function for design generation is:

$$f(x) = a_1 \cos \pi x + \left[ \frac{(a_{21} - a_{22})}{R} x + a_{21} \right] \sin \left[ \left( \frac{(f_2 - f_1)}{R} x + f_2 \right) 2\pi x \right] \quad (12)$$

This method exhibits an increase in problem dimension to six and the plate takes on a trigonometric function profile, which can be optimized via gradient-based methods as a function of six variables. The optimization problem is stated as

$$\begin{aligned} & \text{find} && c, a_1, a_{21}, a_{22}, f_1, f_2 \\ & \text{minimize} && M(c, a_1, a_{21}, a_{22}, f_1, f_2) = \rho A(c, a_1, a_{21}, a_{22}, f_1, f_2) c \\ & \text{subject to} && P_c(c, a_1, a_{21}, a_{22}, f_1, f_2) - P_{c \max} \leq 0 \\ & && x_i^2 + y_i^2 = r_i^2 \\ & && z - a_1 \cos \pi r + \left[ \frac{(a_{21} - a_{22})}{R} r + a_{21} \right] \sin \left[ \left( \frac{(f_2 - f_1)}{R} r + f_2 \right) 2\pi r \right] = 0 \\ & && 7.5 \text{ mm} \leq c \leq 50 \text{ mm} \\ & && h = 120 \text{ mm} \\ & && 0 \leq a_1 \leq h - a_{21} \\ & && 0 \text{ mm} \leq a_{21} \leq 20 \text{ mm} \\ & && 0 \text{ mm} \leq a_{22} \leq 5 \text{ mm} \\ & && 0 \leq f_1 \leq 50 \\ & && 0 \leq f_2 \leq 50 \end{aligned} \quad (13)$$

### 3.5.1 Mesh refinement and two-stage optimization

The complex curvature of the surfaces generated by the trigonometric function design were not able to be rendered with accuracy in the standard  $26 \times 26$  plate used throughout this study. The design can exhibit many small rippling curvatures, which cannot be captured by a course mesh. As shown in Figure 9, an increase in the level of mesh refinement is necessary to obtain valid experimental results.

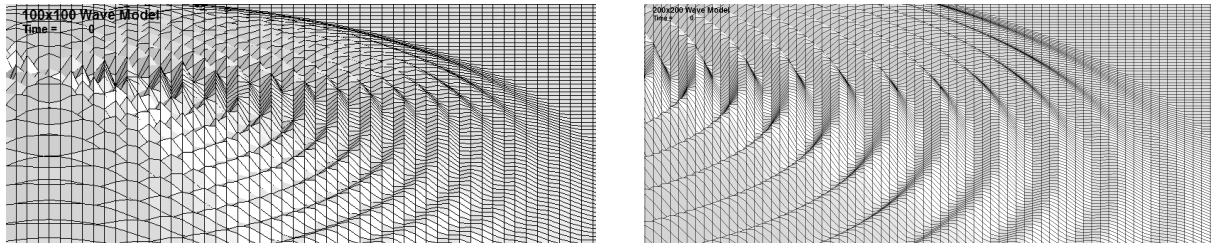


**Figure 9: Detail of plate showing mesh refinement to capture detailed curvature of trigonometric function design method. 100x100 element mesh refinement (left) and 200x200 element mesh refinement (right) are shown.**

Through a mesh convergence study it was found that a  $200 \times 200$  mesh discretization of the design domain was adequate to achieve accurate results. This mesh refinement comes at the cost of dramatically increased computational time however, as the number of elements increases from 625 to 40000. This increase correlates to an increase in FEA simulation time from approximately 5 seconds to over 10 minutes in some cases. When the bounds on the design variables are large, the

number of function calls necessary to find the gradient for optimization can be high, resulting in a convergence time for this optimization problem that is unreasonably high. In order to overcome this problem, the optimization is carried out in two stages of fidelity. A model in which the design domain is discretized into 100 x 100 elements, considered a low-fidelity model with a relatively large error, is used to narrow the bounds to within reasonable spans. After the span of bounds has been reduced, a high-fidelity model is used to find the convergent design. This process resulted in an accurate, convergent design at a fraction of the computational cost.

The convergent design, shown in Figure 10, exhibits some amplitude and frequency modulation of the second trigonometric term, and the plate takes on the appearance of raised concentric ripples emanating from the center of the structure.

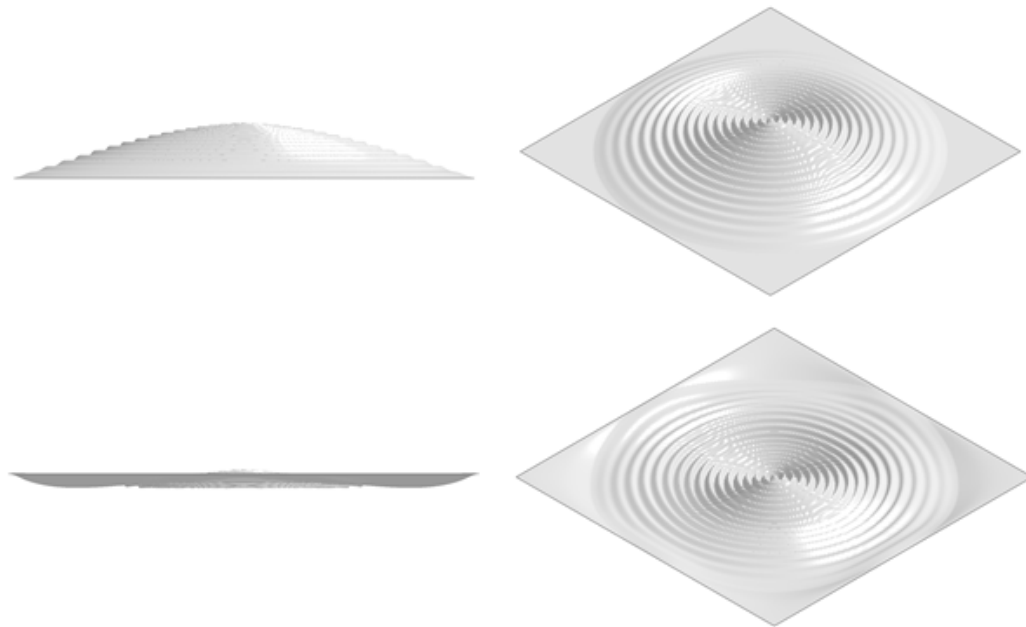


**Figure 10: Finite Element model showing the optimized trigonometric function surface design before (top) and after a blast event (bottom). Convergent numerical results: thickness = 8.31 mm,  $a_1 = 0.1045$ ,  $a_{21} = 0.01549$ ,  $a_{22} = 0.0000$ ,  $f_1 = 44.794$ ,  $f_2 = 34.000$ , mass = 81.2 kg.**

This design method yields the greatest reduction in mass over baseline (-64.1 %) and a substantial reduction in mass over the Gaussian design, the next best performing method (-14.0 %). Despite the increase in the complexity of the curvature, the reduction in mass is due to a thinner structure than was found in previous results. In this case, an increase in the order of the optimization problem allowed for a more pronounced relaxation of the design, and resulted in a higher performance, more complex structure.

## 4 FREE SHAPE DESIGNS

### 4.1 Inverted Profile Design

There has been some interest in creating a plate that takes on an inversion of the topography of a flat plate after a blast event. The reasoning being that the complex blast pressure distribution would then determine the shape of the plate and increase the  $z$ -coordinate at each proportional to the magnitude of the loading. The basic procedure used to generate the topography for this plate is as follows:

- Expose a flat plate of some thickness  $c$  to a blast event of time  $t = t_c$  in order to capture the maximum deflection caused by the blast.
- Invert the shape about the  $xy$ -plane for all nodal locations.
- Scale all  $z$  values to remain within the design space (if necessary).

Through the execution of this procedure, the topography of the plate is determined without the application of any rigorous analytical description. This inversion procedure allows the designer to create complex shapes proportional to the loading condition without the need for complicated analytical descriptions that would not be feasibly solvable by traditional gradient-based optimization methods. After the inversion procedure, the topography of the plate is fully specified, and the design is optimized via the active-set algorithm used to find the convergent results for the geometrically constrained designs in the previous sections. The objective function is a single variable function where only the thickness of the plate structure is allowed to vary:

$$\begin{aligned} & \text{find} && c \\ & \text{minimize} && M(c) = \rho A c \\ & \text{subject to} && P_c(c) - P_{c \max} \leq 0 \\ & && 7.5 \text{ mm} \leq c \leq 50 \text{ mm} \end{aligned} \tag{14}$$

The optimized design, shown in Figure 11, exhibits a performance increase over the baseline design in terms of mass reduction very similar to the geometrically constrained designs but with an optimization problem of order one, whose solution can be found with much less computation. In addition, it utilizes the entire square area of the design domain and could easily be applied to irregularly shaped design domains with little difficulty.

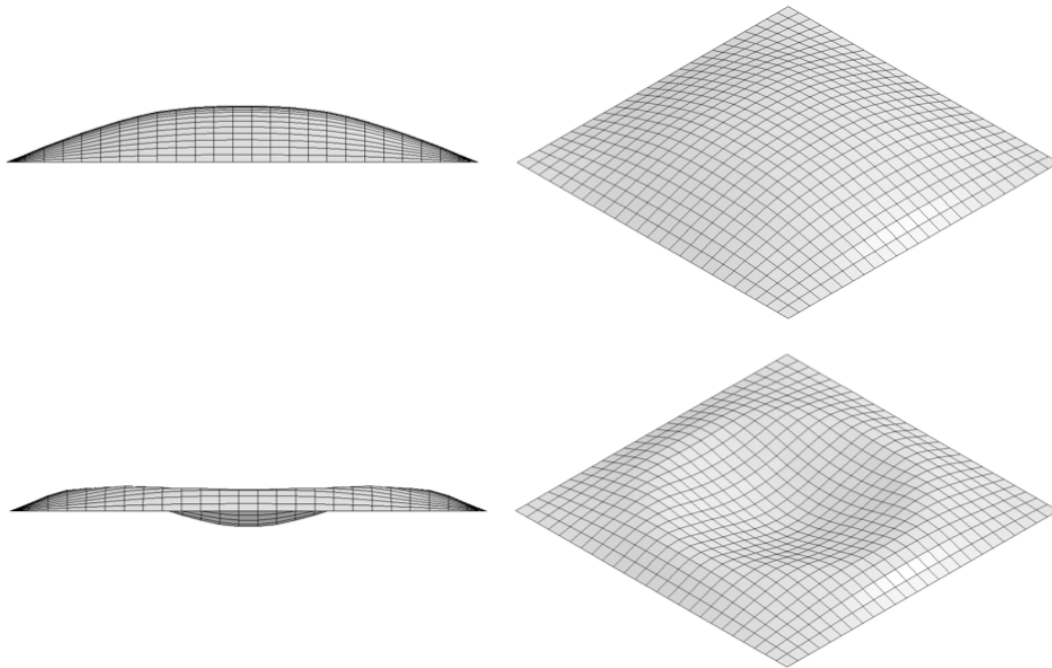


**Figure 11: Finite Element model showing the optimized inverted profile design before (top) and after a blast event (bottom). Convergent numerical results: thickness = 13.6 mm, mass = 105.8 kg.**

## 4.2 HCA Topography Design

The HCA topography design is an alternative free shape design method, which allows for the generation of complex curved structures without the need for complex analytical description. The HCA algorithm considers the nodal z-coordinates of all unconstrained nodes in the design domain at every iteration. Thus, the objective function is of dimension  $N$ , where  $N$  is the total number of free nodes in the design domain. The convergence behavior is such that the shape depth is increased incrementally at each iteration of the control-based HCA algorithm until the penetration constraint is satisfied. The thickness of the plate is fixed, and the objective function  $M$ , is purely a function of the plate geometry. The optimizer does not evaluate the mass at every iteration, but simply iterates until the constraints are met. Given an initially flat surface (all nodal locations  $\tilde{z} = 0$ ) and a fixed elemental thickness ( $c = c_i$ ), the HCA algorithm is applied to the design domain iteratively until convergence criteria as fixed by the designer are met.

After preliminary analysis, a thickness of  $c_i = 12.2$  mm was chosen in order to keep the structure as lightweight as possible while utilizing the entire design domain without violating deflection constraints. The final design obtained from the nodal HCA algorithm is given in Figure 12 below, with the resulting parameter information given.

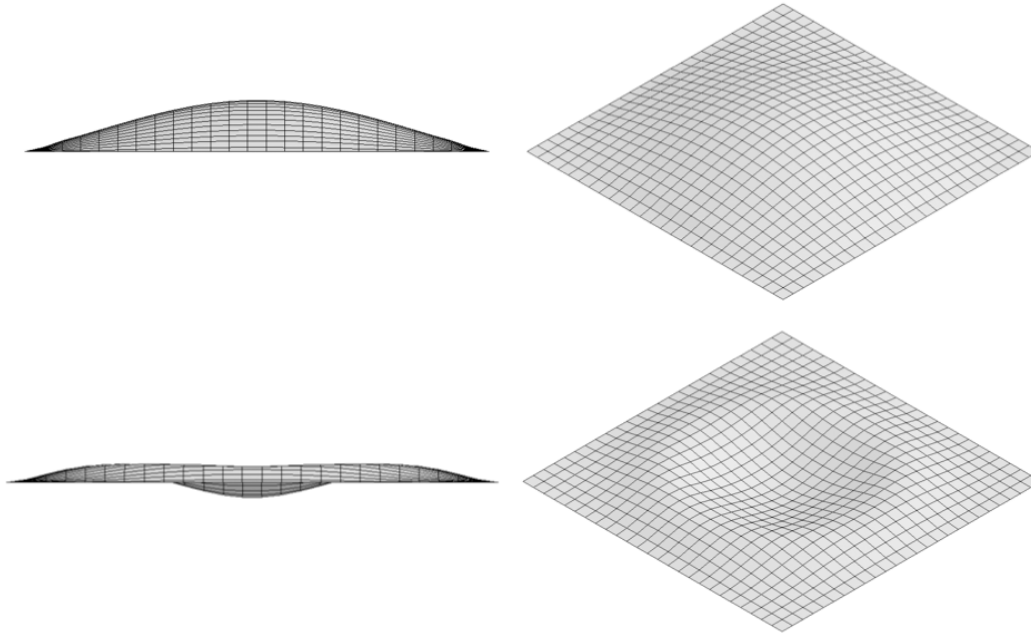


**Figure 12: Finite Element model showing the optimized HCA profile design before (top) and after a blast event (bottom). Numerical results: thickness = 12.2 mm, structure height = 11.9 mm, mass = 97.8 kg.**

To demonstrate the dependence of the converged solution on user inputs, a second design is generated using an initial starting thickness of  $c_i = 0.015$  m. This second structure satisfies the same penetration constraint with a lower height, while exhibiting an increase in mass. In other words, the plate is designed to be thicker and have more mass with the trade-off that it takes up less space in the vertical direction, demonstrating the high-level of control the designer can maintain in the customization of the structure. Table 2 shows the comparative results.

**Table 2: Numerical comparison of HCA profile designs 1 and 2.**

| <b>Trial</b> | <b>Thickness (mm)</b> | <b>Height of Structure (mm)</b> | <b>Mass (kg)</b> |
|--------------|-----------------------|---------------------------------|------------------|
| HCA Design 1 | 12.2                  | 11.9                            | 97.8             |
| HCA Design 2 | 15.0                  | 8.61                            | 118.7            |

While the geometrically constrained candidate designs can be optimized with gradient-based methods, this approach is not feasible for the HCA objective function due to the large dimensional order of the optimization problem. Convergence criteria must instead be chosen by the designer based on specific performance goals and the application of the structure. In addition, the design rules are extremely problem dependent and are determined through algorithmic testing. Despite the problems of demonstrating convergence and the heuristic nature of the design, the HCA method exhibits some key advantages over geometrically constrained designs: computational efficiency and a broad potential for application to irregular design domains.

#### 4.2.1 Design algorithm

The hybrid cellular automaton (HCA) method combines the basis of the cellular automaton (CA) paradigm, introduced by Stanislaw Ulam and John von Neumann in 1950s [16], and the theory of finite element-based structural optimization, introduced by Lucien Schmit in 1960s [17]. The HCA method presented by Tovar, et al. [18] incorporates local updating schemes such as control rules (i.e., on-off, proportional, integral and derivative controllers and ratio techniques). These local rules drive a defined field variable to an optimum state or set point. The expression for the field variable and the value of the set point are derived from the optimality conditions of the structural design problem [19]. A proof of the global convergence of the HCA technique, under certain circumstances, to an optimal design has been derived [1].

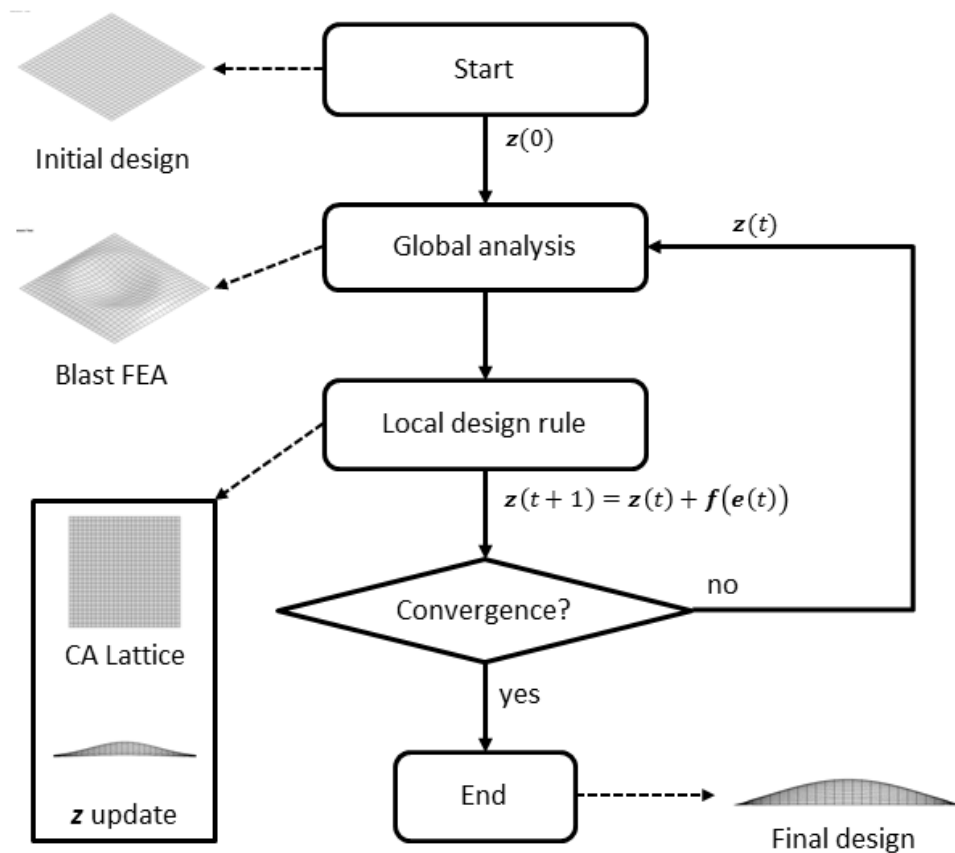


**Figure 13: HCA algorithm process flow diagram showing plate structure application.**

The HCA algorithm as applied to the plate topography problem is illustrated in Figure 13 above. This methodology assumes that cellular automata (CAs) form a structure or design domain, and sensors and actuators within the CAs activate local formation and resorption of material. With a proper control strategy, this process drives the overall structure to an optimal topography by updating the nodal locations. Using distributed controlled rules, the optimization problem can be stated as

$$\begin{aligned}
& \text{find} && \mathbf{z} \\
& \text{minimize} && |q^* - q_{min}| \\
& \text{subject to} && |q_{min}| - P_c \max \leq 0 \\
& && \mathbf{z}^L \leq \mathbf{z} \leq \mathbf{z}^U
\end{aligned} \tag{15}$$

where  $\mathbf{z}$  is the set of all nodal coordinate values associated the plate topography. In (15)  $q^*$  is the target deflection threshold value to be achieved by every element in the structure. The iterative approach may be achieved using a control-based algorithm or a ratio approach. A control-based approach is implemented to perform topography optimization as shown in Figure 14. Multiple gains ( $K_\alpha$  and  $K_\beta$ ) allow the designer control over the rate at which the topography of the structure is updated.

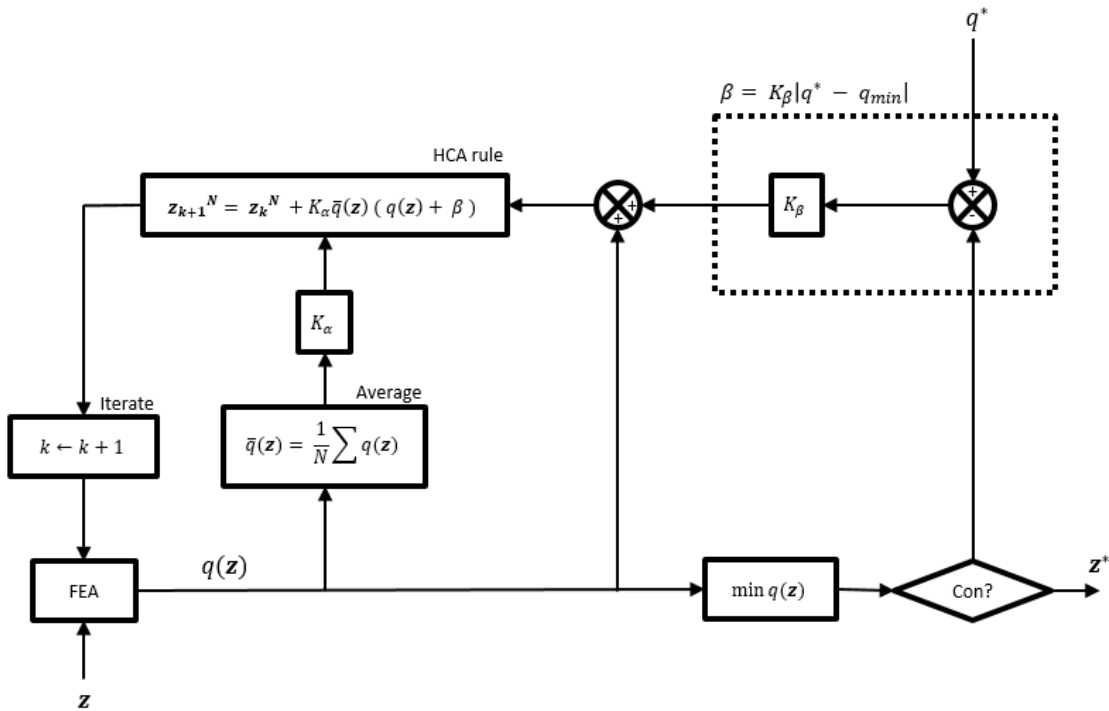


Figure 14: Control-based strategy for updating nodal locations to optimize topography.

#### 4.2.2 Computational efficiency and convergence considerations

The computational efficiency of the HCA topography design is rooted in two key characteristics of the design method. The first is the relative insensitivity to mesh refinement. Due to the nature of the shape produced by HCA topography a fairly coarse mesh can be used to generate structures, as opposed to some of the more complex geometrically constrained design methodologies, which require a higher level of mesh refinement for modeling accuracy. A mesh convergence study performed on the HCA method demonstrated nearly identical results for models containing 625 elements and 40000 elements in terms of mass and deflection.

*Table 3: HCA mesh convergence study results.*

| <b>Grid size</b> | <b>Number of elements</b> | <b>Mass of converged design (kg)</b> |
|------------------|---------------------------|--------------------------------------|
| 25 x 25          | 625                       | 97.8                                 |
| 100 x 100        | 10000                     | 98.1                                 |
| 200 x 200        | 40000                     | 98.1                                 |

In addition to the relatively low mesh requirements, the HCA method is in general more computationally efficient in that it only requires one function call per iteration, independent of the number of design variables. Gradient-based optimization methods can require many function calls, in some cases hundreds per iteration to determine the gradient and hessian matrices for higher-dimension optimization problems. In the case of structure design, these multiple function calls to FEA simulation can be very computationally expensive. This benefit is augmented by the controls-based optimization routine, which allows the designer to control the rate of convergence through gain adjustments in the control rule.

#### 4.2.3 Application to irregular design domains

The other primary advantage of the HCA topography has over the geometrically constrained designs is its potential for much broader application to irregular design domains. While some of the geometrically constrained designs are dependent on symmetric bounds (e.g. the pyramid profile design) and others fail to take advantage of the entire design domain due to their inherently circular footprint (e.g. the polynomial and trigonometric function designs), the HCA can be applied without difficulty to a wide range of design domains under vastly different loading and support conditions. Figure 15 below demonstrates the adaptation of the HCA method to an irregular design space meant to simulate the under-armor of a vehicle.

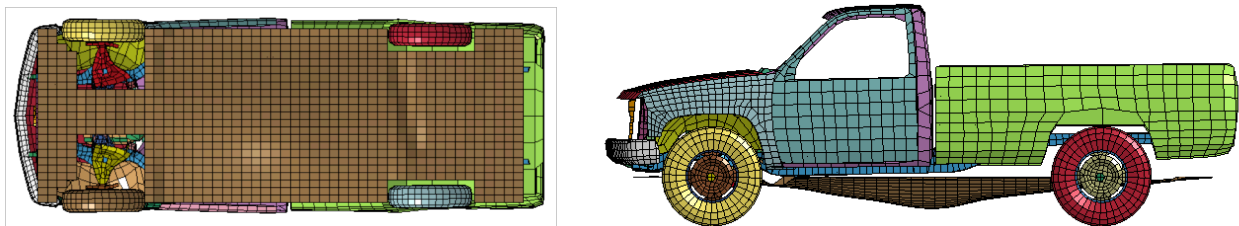


*Figure 15: HCA topography design in application to under-vehicle design domain. The domain is shown from the bottom of the vehicle (left) and the convergent design is shown in application from the right (right).*

## 5 COMPARATIVE NUMERICAL RESULTS

The numerical results of the convergent designs are divided into two tables in order to compare only designs operating within the same design domain. Table 4 contains performance values for the radial design domain methods. Table 5 contains performance values for the full design domain methods. In both design domain cases, radial and full, there is a trend of increased performance in terms of mass reduction as the number of design variables increases.

*Table 4: Comparative numerical results: radial design domain*

| Method                        | No. of design variables | No. of iterations | No. of function calls | Mass of converged design (kg) | Mass reduction from baseline (%) |
|-------------------------------|-------------------------|-------------------|-----------------------|-------------------------------|----------------------------------|
| Flat Plate Design             | 1                       | 18                | 71                    | 226.4                         | 0.0                              |
| Polynomial Function Design    | 5                       | 173               | 1398                  | 113.1                         | -50.0                            |
| Trigonometric Function Design | 6                       | 272*              | 1723*                 | 81.2                          | -64.1                            |

\* These totals are a sum of the iterations necessary for the high and low fidelity models to converge

*Table 5: Comparative numerical results: full design domain*

| Method                   | No. of design variables | No. of iterations | No. of function calls | Mass of converged design (kg) | Mass reduction from baseline (%) |
|--------------------------|-------------------------|-------------------|-----------------------|-------------------------------|----------------------------------|
| Flat Plate Design        | 1                       | 18                | 71                    | 226.4                         | 0.0                              |
| Pyramid Profile Design   | 2                       | 17                | 121                   | 99.1                          | -56.2                            |
| Gaussian Function Design | 3                       | 9                 | 82                    | 94.3                          | -58.4                            |
| Inverted Profile Design  | n/a**                   | n/a               | n/a                   | 105.8                         | -53.3                            |
| HCA Topography           | N***                    | 112               | 112                   | 97.8                          | -56.8                            |

\*\* The procedure of inverting the shape does not apply to the computational efficiency of the design method

\*\*\* N is equal to the number of free nodes in the design domain

As was stated previously, the validation of HCA concept designs can be extremely problematic, but an attempt is made here to accomplish validation through direct comparison to benchmark results. The summary of numerical results as an improvement of the baseline design is given in Table 5. In every case, the penetration for the converged design is zero. The comparative numerical results for the HCA method demonstrate a substantial performance improvement over the baseline design in terms of mass reduction and performance approximately equal to or better than all converged candidate designs, with the exception of the trigonometric function design method. These results demonstrate the success of the HCA topography design in generating structures of

equal and in some cases superior to geometrically constrained designs while using fewer computational resources and allowing the designer a higher degree of control.

## 6 CONCLUSIONS

In this work, the topography optimization of isotropic steel plate structures to mitigate blast loading is accomplished. Several design strategies are examined, falling under two categories: geometrically constrained designs, whose shape is bound to analytical definition, and free space designs, whose shape is allowed to change freely under the control of the optimization algorithm. In the optimization problem applied to all designs, the mass of the structure is minimized while deflection constraints are met. Through this comparison study, it is possible to draw some conclusions about the success of the various methods to produce good candidates for blast protection design.

Through optimization of topography, all designs exhibit an increase in performance in terms of mass reduction over baseline while maintaining an allowable amount of deflection. Optimum designs found through an expansion of the order of the optimization problem from one to six demonstrated a general trend of increased performance as the domain constraints are relaxed and the design is able to assume more complex analytical shapes. Numerical results of convergent designs based on trigonometric functions demonstrate a reduction in mass of 64% over baseline. This result exceeds all other performance results for the various designs and makes the trigonometric function design a good candidate for further study, especially the potential to apply the methodology to irregular design spaces and the sensitivity of the design to variations in loading conditions. Future research is indicated in the development of a robust design rooted in this trigonometric function design method.

It is problematic to prove a global optimum with HCA and other free space methods, as their method of optimization is not based on KKT conditions. However, designs generated via the Hybrid Cellular Automata (HCA) topography method resulted in structures whose performance paralleled or exceeded most geometrically constrained designs despite the fact that they can be created with fewer computational resources and adapted easily to irregular design domains. Under well-chosen control gains, the HCA method can produce designs similar in quality to that of designs produced by gradient-based optimization methods using hundreds of fewer function calls.

The primary disadvantage of this type of empirical model for blast loading is the absence of reflective waves from surrounding surfaces, i.e., the ground, buildings, etc. Future studies should include MM-ALE or similar solver to account for fluid-material interactions and include those effects. Much attention has been paid recently to the development of sandwich structures as a multi-material approach to blast mitigation problems and some have demonstrated significant reduction of stress amplitude, especially through the use of honeycomb structures. Future work will incorporate concurrent material and shape optimization, and if possible will include the application of the design candidates examined here to multiple-material design.

## 7 ACKNOWLEDGEMENTS

This material is based upon work supported by the U.S. Army TACOM Life Cycle Command under Contract No. W56HZV-08-C-0236, through a subcontract with Mississippi State University and the University of Notre Dame, and was performed for the Simulation Based Reliability and Safety (SimBRS) research program. Any opinions, findings, conclusions, and recommendations expressed in this paper are those of the writers and do not necessarily reflect the views of the sponsors.

## 8 REFERENCES

1. Goetz, J., et al., *Two-material optimization of plate armour for blast mitigation using hybrid cellular automata*. Engineering Optimization, 2012. **44**(8): p. 985-1005.
2. Argod, V., et al., *Shape optimization of solid isotropic plates to mitigate the effects of air blast loading*. Mechanics Based Design of Structures and Machines, 2010. **38**(3): p. 362-371.
3. Wang, H., et al. *Function-Oriented design of innovative composite materials for high speed impact*. in *Materials Science and Technology Conference and Exhibition, MS and T'07 - "Exploring Structure, Processing, and Applications Across Multiple Materials Systems"*, September 16, 2007 - September 20, 2007. 2007. Detroit, MI, United states: Curran Associates Inc.
4. Jiang, D., et al., *Innovative composite structure design for blast protection*, in *SAE World Congress 2007*, US Army RDECOM-TARDEC: 6501 E 11 Mile Rd Warren MI 48397-5000.
5. Tan, P.J., et al., *Dynamic compressive strength properties of aluminium foams. Part II - 'shock' theory and comparison with experimental data and numerical models*. Journal of the Mechanics and Physics of Solids, 2005. **53**(10): p. 2206-2230.
6. Hanssen, A.G., et al. *Close-range blast loading of aluminium foam panels: A numerical study*. in *IUTAM Symposium on Mechanical Properties of Cellular Materials, September 17, 2007 - September 20, 2007*. 2009. Cachan, France: Springer Verlag.
7. Randers-Pehrson, G. and K.A. Bannister, *Airblast loading model for DYNA2D and DYNA3D*, 1997: Army Research Laboratory.
8. Kuhl, A.L., *Dynamics of detonations and explosions - explosion phenomena*, 1991, American Institute of Aeronautics and Astronautics: Washington, D.C.
9. Hirt, C.W., A.A. Amsden, and J.L. Cook, *An arbitrary lagrangian-eulerian computing method for all flow speeds*. Journal of Computational Physics, 1974. **14**: p. 227-253.
10. Joynt, V.P., *Mine Resistant Armored Vehicle*, 2008, Force Protection Industries, Inc. (Ladson, SC, US): United States.
11. Tan, H., *Vehicle Hull Shape Optimization for Minimum Deformation Under Blast Loading* 2010.
12. Troyano, L.F., *Bridge Engineering: A Global Perspective*. 2003: Thomas Telford.
13. Osserman, R., *How the Gateway Arch Got its Shape*. NEXUS NETWORK JOURNAL, 2010. **12**(2): p. 167-189.
14. Ngo, T., et al., *Blast loading and blast effects on structures - An overview*. Electronic Journal of Structural Engineering, 2007. **7**: p. 76-91.

15. Powell, M.J.D., *A Fast Algorithm for Nonlinearly Constrained Optimization Calculations*. Numerical Analysis, 1978. **Vol. 630**.
16. Wolfram, S., *A New Kind of Science* 2002, Champaign, IL: Wolfram Media. 1197.
17. Schmit, L.A., *Some approximation concepts for structural synthesis*. AIAA Journal, 1974. **12**: p. 692-699.
18. Tovar, A., et al., *Topology Optimization Using a Hybrid Cellular Automaton Method with Local Control Rules*. ASME Journal of Mechanical Design, 2006. **128**(6): p. 1205-1216.
19. Tovar, A., et al., *Optimality Conditions of the Hybrid Cellular Automata for Structural Optimization*. AIAA Journal, 2007. **45**(3): p. 673-683.